

Batteries & Supercaps

 **Chemistry
Europe**
European Chemical
Societies Publishing

Accepted Article

Title: Stable Long-Term Cycling of Room-Temperature Sodium-Sulfur Batteries Based on Non-Complex Sulfurised Polyacrylonitrile Cathodes

Authors: Jesús M. Blázquez-Moreno, Ana L. Páez Jerez, Alvaro Y. Tesio, Almudena Benitez, and Alvaro Caballero

This manuscript has been accepted after peer review and appears as an Accepted Article online prior to editing, proofing, and formal publication of the final Version of Record (VoR). The VoR will be published online in Early View as soon as possible and may be different to this Accepted Article as a result of editing. Readers should obtain the VoR from the journal website shown below when it is published to ensure accuracy of information. The authors are responsible for the content of this Accepted Article.

To be cited as: *Batteries & Supercaps* **2024**, e202400640

Link to VoR: <https://doi.org/10.1002/batt.202400640>

*Stable Long-Term Cycling of Room-Temperature Sodium-Sulfur Batteries
Based on Non-Complex Sulfurised Polyacrylonitrile Cathodes*

Jesús M. Blázquez-Moreno,^a Ana L. Páez Jerez,^b Alvaro Y. Tesio,^{a,b,*} Almudena Benítez,^{a,*} Álvaro Caballero^a

^a Dpto. Química Inorgánica e Ingeniería Química, Instituto Químico para la Energía y el Medioambiente (IQUEMA), Universidad de Córdoba, Campus de Rabanales, Córdoba, 14014, Spain.

^b Centro de Investigación y Desarrollo en Materiales Avanzados y Almacenamiento de Energía de Jujuy (CIDMEJu), Centro de Desarrollo Tecnológico General Manuel Savio, Palpalá, Jujuy, 4612, Argentina.

*Corresponding authors: q62betoa@uco.es (A. Benítez); Tel.: +34–957218620; atesio@cidmeju.unju.edu.ar (A.Y. Tesio)

Abstract

The cost-effectiveness and high theoretical energy density make room-temperature sodium-sulfur batteries (RT Na–S batteries) an attractive technology for large-scale applications. However, these batteries suffer from slow kinetics and polysulfide dissolution, resulting in poor electrochemical performance. Thus, the sulfurised polyacrylonitrile (SPAN) cathode is postulated as a suitable material due to the retention of sulfur through covalent bonds and the increase in the conductivity of sulfur. Furthermore, in this work the synthesis of SPAN has been carried out using simple synthesis methods, making it scalable, economical, and without the use of toxic compounds. The incorporation of the SPAN material helps mitigate the shuttle effect, reducing the capacity loss and improving both the efficiency and lifespan of Na–S batteries. The SPAN-based cathode demonstrates that this RT Na–S battery configuration shows high stability, reaching 1000 cycles with a capacity loss per cycle of 0.11% and a satisfactory specific capacity of 400 mAh/g_s at a high rate of 2C. This study demonstrates that the utilisation of SPAN derived from a non-complex synthesis can be a viable alternative for enhancing the future of Na–S batteries technology.

Keywords: sodium-sulfur batteries; sulfur-polyacrylonitrile cathode; ultra-long cycling; mechanochemical synthesis.

1. Introduction

The rapidly growing need for energy storage exceeds the energy density of the currently dominant commercial lithium-ion batteries (~ 200 Wh/kg).^[1] Therefore, there is an exhaustive search to find a viable alternative to lithium-ion batteries. Thus, metal-sulfur technology is strongly emerging as the next-generation of rechargeable batteries. In particular, lithium-sulfur (Li-S) and sodium-sulfur (Na-S) batteries are gaining attention because of their high theoretical gravimetric energy density, 2615 Wh/kg as well as the low cost and non-toxicity of sulfur.^{[2][3]} Sodium is more abundant and less expensive than lithium, making it an attractive alternative for large-scale energy storage applications. The sodium content in both the Earth's crust and water are 28400 mg/kg and 1000 mg/L, respectively, compared to 20 mg/kg and 0.18 mg/L for lithium. Therefore, the characteristics of sulfur make it an ideal element to be used as a cathode, for the development of low-cost, high-energy density, and eco-friendly systems.^[4]

The first Na-S battery was developed in the 1960s using sodium as the anode and sulfur as the cathode, separated by a solid β -alumina ceramic electrolyte,^[5] operating at 300 °C. However, the high working temperature results in a loss of electrical energy, major safety concerns, and cell degradation.^[6] Therefore, to avoid the aforementioned issues, research has focused on manufacturing room-temperature (RT) Na-S batteries. The RT Na-S battery, like its Li-S counterpart, can reach a theoretical capacity of 1675 mAh/g through a series of processes. These processes include the complete conversion of all long-chain polysulfides (PS) to Na₂S, the solvation/desolvation of Na⁺ ions in the electrolyte, as well as the plating/stripping of Na on the anode.^[7]

In addition to the inherent challenges of Li–S batteries, such as the insulating nature of sulfur and the shuttle effect, RT Na–S batteries still face their own issues of sluggish kinetics and low capacity.^[7] To address these problems, conductive matrices are used that facilitate the electron mobility, thus improving the overall electrochemical performance of the cell. In this way, a previously reported useful matrix is the carbonaceous matrix that allows the effective accommodation of sulfur becoming crucial to prevent the dissolution of long-chain polysulfides, which are responsible for the shuttle effect.^[8,9] Various carbon-based materials have been widely investigated in the literature, including carbon nanotubes,^[10] carbon nanofibers,^[11] biomass-derived carbons,^[12,13] or conductive carbon polymers.^[14] An effective strategy to address the challenge of the shuttle effect is to use materials where sulfur is covalently bonded to the cathode matrix.^[15] Among the latter, polyacrylonitrile (PAN) is a polymer capable of anchoring sulfur to the polymer chain through a simple synthesis, avoiding the dissolution of polysulfides in the electrolyte, and improving both stability and cell capacity. Within this context, a promising category of materials called sulfurised polyacrylonitrile (SPAN) emerges as a potential breakthrough, which could be the key to unlocking the full potential of sodium-sulfur batteries, even at room-temperature.^[16,17]

In 2002, Wang et al. pioneered the development of the first sulfurised polyacrylonitrile (SPAN) cathode, which has since demonstrated remarkable success as a cathode material in rechargeable Li–S batteries.^[18–21] In contrast, the applicability of SPAN cathodes in RT Na–S batteries is relatively limited, with only a handful of articles available in the literature. The most widely used electrolytes are based on carbonated solvents, either with or without the addition of fluoroethylene carbonate (FEC) and the average sulfur mass loading was $\leq 1 \text{ mg/cm}^2$.^[22–26] Only Wang et al. reported an area mass loading of up to 4.5

mg/cm²; however, this achievement was limited to only 18 cycles and a low C-rate (0.013C).^[27] According to some authors, freestanding cathodes with respectable electrochemical performances were claimed to exist without the need for binders and/or conductive additives.^[10,11,14,24,28] The longest cycling was achieved by preparing electrodes with 20 wt.% of conductive agent and on carbon-coated aluminium foil as the current collector, specifically cycling 600 and 1000 charge and discharge cycles.^[25,26] Notably, the greatest results so far were reported by Murugan and co-workers, whose SPAN cathode with a sulfur content of 38.18 wt.% showed remarkably high capability at current densities ranging from 1 to 10 C. Surprisingly, the same cathode reached a stable cycling for 1000 cycles, maintaining a capacity value of 1072 mAh/g at 3C, but using as electrolyte a sodium salt synthesised with laborious synthesis methods and a low sulfur content in the cathode.^[29] However, the synthesis of SPAN in these works is carried out using high temperatures of up to 550 °C and high nitrogen flows of 200 L/h, as well as the use of organic solvents such as toluene to make a Soxhlet extraction, which makes the synthesis less affordable and scalable at an industrial level.

In this work, we report an effective SPAN cathode for RT Na–S batteries. Non-complex synthesis of the SPAN material is conducted through a wet mechanochemical treatment combined with pyrolysis at low temperature. This method introduces a significant content of sulfur into the polyacrylonitrile polymeric chain, creating covalent bonds between carbon and sulfur. As a result, the dissolution of long-chain polysulfides is prevented, leading to a significant improvement in electrochemical performance and a reduction in the shuttle effect, demonstrated by the good stability shown even at 1000 cycles, providing a specific capacity of about 200 mAh/g at C/5 rate. Additionally, at high current densities, such as 2C,

considerable capacity values are maintained, recovering later the initial capacity when cycling again at slow rates. Therefore, SPAN-type materials are versatile and easy to synthesise, making them an attractive option for large-scale commercialisation. Also, we have minimized the use of raw materials, employing only 10% of the conductive agent in the cathode preparation. Likewise, for the electrolyte formulation, we avoided using salts synthesized through complex methods and did not incorporate high-cost additives like fluoroethylene carbonate (FEC). With further research and development, these materials could revolutionise the field of energy storage, paving the way to a more sustainable and green future.

2. Results and discussion

2.1. SPAN characterisation

SPAN was prepared by a heating process mixing PAN and elemental sulfur, where sulfur was incorporated into the polymer chain. To quantify how much sulfur was anchored to the polymer, an elemental analysis was performed, as shown in Table 1. In this analysis, a sulfur content of 34 wt.% was obtained, which was slightly lower than what is commonly found in the literature, as shown in Table S1. However, the percentage of active material is similar to literature for other SPANs synthesised by more complex techniques such as electrospinning, or others obtained at higher synthesis temperatures.^[22,29] Additionally, it is important to determine the form in which the sulfur is present in the compound, whether the S is covalently bonded to the polymer chain or in its elemental form S₈. It is noteworthy that the nitrogen content was 10.7 wt.%, which has proven to be a highly effective electrocatalyst to prevent the dissolution of polysulfides in the electrolyte.^[30]

Table 1. Elemental analysis of SPAN

Sample	Carbon (wt.%)	Nitrogen (wt.%)	Sulfur (wt.%)
SPAN	28.7	10.7	34.1

In general, the sulfur present in SPAN is covalently bonded to the carbonaceous backbone of the polymer (e.g., C–S, N–S), in addition to the semi-elemental S found in chains of S–S bonds of various lengths. The local environment of these types of sulfur introduces significant differences in thermal decomposition behaviour. When this sulfur is covalently attached to the PAN backbone chain, decomposition occurs at higher temperatures.^[31] Therefore, to draw conclusions regarding the chemical nature of the sulfur in SPAN, thermogravimetric analysis (TGA) was performed under inert atmosphere, as illustrated in Figure S1a. The first noticeable weight loss of around 10% occurs in the temperature range of 220 – 360 °C, corresponding to the sublimation of sulfur that is physically confined inside the polymeric structure. This type of sulfur could be found in the form of short chains of about 2 – 4 atoms.^[32] Subsequently, the second loss occurs from 360 to 650 °C, corresponding to the degradation and sublimation of SPAN, including both C–S and N–S bonds, as well as the polymer chain. This loss is the most substantial, representing approximately 65% of the total. The sublimation of sulfur, which is covalently bonded to the polymeric chain, and its degradation overlap in this temperature range, which makes it difficult to precisely quantify the sulfur content with TGA analysis.^[22,33] It can be observed that above 700 °C, there is no further thermal degradation of the material, leaving the TiO₂ additive and residues uncarbonized.^[34] In contrast, the TGA of sulfur powder exhibits a sharp weight loss around 155 °C, a temperature at which elemental sulfur sublimates. It is worth

noting that sulfur not covalently bonded to the polymeric PAN chain is lost at a higher temperature with respect to pristine sulfur, confirming its physical confinement within the polymer or its attachment to side chains of the polymeric carbon. [33]

Additionally, a TGA-MS analysis was conducted to assess at which temperature range degradation processes occur (Figure 1a). [35] It was observed that the mass-to-charge ratio (m/z) of 64, corresponding to sublimated S_2 ; detection begins at temperatures above 220 °C. This type of sulfur corresponds to the sublimation of sulfur physically confined within the polymeric structure, as evidenced by the initial weight loss in the TGA. Subsequently, at a higher temperature range starting from 400 °C, m/z ratios of 30 and 44, associated with NO and CO_2 elements, respectively, begin to be detected. These elements originate from the degradation of the polymeric chain of SPAN, as observed in the TGA curve. It is noteworthy that, although the synthesis was carried out at a low temperature, the m/z 34 signal relative to the release of H_2S was not observed in the MS spectra, confirming the complete cyclisation reaction as reported by Buchmeiser et al. [35] Notably, within the same temperature range, the presence of sulfur bonded covalently with the polymeric structure is detected, alongside the release of S_2 . [35] Regarding the calculation of the fraction of sulfur covalently bound to the polymer chain, two complementary characterization techniques (EA and TGA) were employed, and the results were in good agreement. Firstly, elemental analysis of the SPAN sample revealed a total S content of 34 wt.%. In the TGA profile for SPAN sample (Figure S1a), an initial weight loss of approximately 10 wt.% was attributed to physically sorbed sulfur. Consequently, it can be estimated that 24 wt.% of the total sulfur (34 wt.% S determined by EA) is covalently bonded to the polymer. Therefore, this value corresponds to 71 wt.% of covalent sulfur present in the SPAN sample relative to the total S content.

Similarly, analysis using mass spectrometry (TGA-MS) allowed the identification of the m/z 64 fraction, corresponding to the S₂ signal, which exhibited two predominant signals. The first, with a smaller area, appears at temperatures between 250 and 400 °C, corresponding to physically sorbed sulfur. The second, with a larger area, occurs at temperatures between 600 and 850 °C, corresponding to sulfur covalently bound to the polymeric chain. As illustrated in Figure S1b, the integration of the area under the curve demonstrates that 25 wt.% of the S is physisorbed, while 75 wt.% is covalently bound, which is consistent with the previous TGA and EA calculations. To remove sulfur that has not been reacted or physically confined, it is reported in the literature that it can be eliminated through a washing step by the Soxhlet method.^[33] However, in the present study, nothing has been done to avoid the use of toxic organic solvents such as toluene or prevent the generation of liquid synthesis waste that would reduce the environmental sustainability of the process.

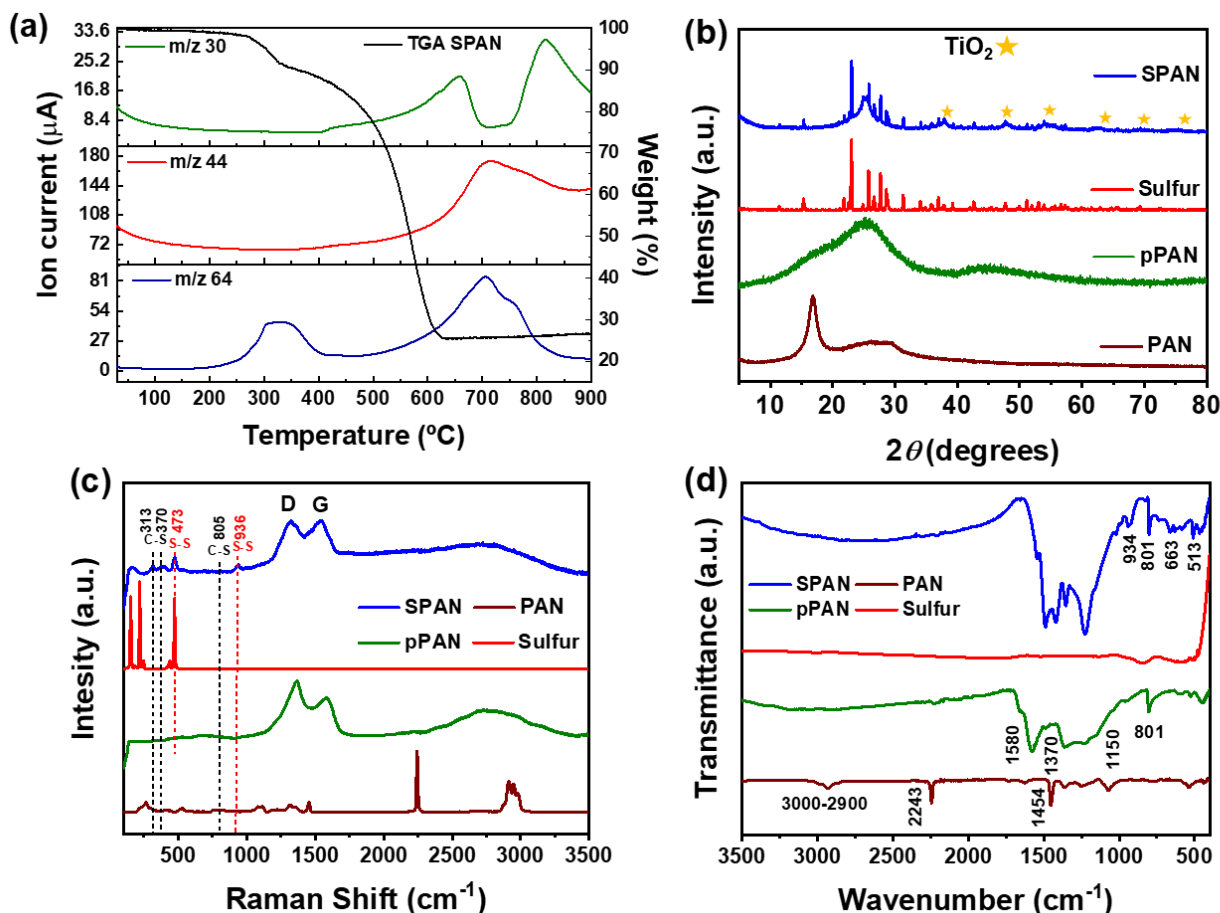


Figure 1. (a) TGA-MS curves under inert atmosphere of SPAN; (b) XRD patterns; (c) Raman spectra; and (d) ATR-FTIR of SPAN, pPAN, PAN and sulfur.

To study the structural composition, the materials were characterised by x-ray diffraction (XRD), Raman spectroscopy, and attenuated total reflection Fourier transform infrared (ATR-FTIR). Figure 1b shows the diffractograms of pristine PAN, pyrolysed PAN (pPAN), elemental sulfur, and synthesised SPAN. The XRD pattern of the bare PAN exhibited a main signal at $2\theta = 17^\circ$ and 29.5° , corresponding to the (110) and (200) planes of PAN crystal structure, respectively.^[36] The XRD pattern of the pPAN sample demonstrates that during the calcination in nitrogen atmosphere of the pristine PAN, this material undergoes an amorphisation and carbonisation process. Two wide and low intensity signals

can be observed in the diffractogram of this product, corresponding to the crystallographic planes (002) and (100) of graphite (Pattern Diffraction File, PDF # 41-1487), reflecting the loss of crystallinity acquired by the carbon material after the calcination process. [22,37] The diffractogram for elemental sulfur revealed the multiple crystallographic planes characteristic of orthorhombic sulfur (PDF # 85-0799), while for the SPAN sample, the diffractogram appeared as a mixture between the pPAN and elemental sulfur samples. Despite the low crystallinity of the carbon formed in the SPAN polymer chain, the main signal at 25° continues to be primarily observed, while simultaneously detecting signals corresponding to highly crystalline sulfur. This shows that a small portion of the elemental sulfur has not been covalently introduced into the polymer structure, confirming the discussion of the results obtained through TGA. In addition, the XRD pattern of SPAN shows several signals (marked with asterisk) that correspond to TiO_2 [PDF# 894203], as reported in the literature. [34,38]

Raman spectra are shown in Figure 1c. In the spectrum of sulfur, the expected signals were observed below 500 cm^{-1} . Specially, three peaks centred at 152, 218, and 472 cm^{-1} could be attributed to the vibration of the S–S bonds of S_8 . [22,39] In the case of the spectrum of the SPAN sample, the peaks located at 152 and 218 cm^{-1} were not observed; however, the peak at 472 cm^{-1} did appear, but with much less intensity, as shown in the inset. This indicates that the majority of the sulfur is located within the carbonaceous structure, although not entirely. Based on the literature, the peaks observed at 313, 370, 394, and 805 cm^{-1} in the spectrum of SPAN correspond to the vibration of C–S bonds, corroborating the presence of covalent bonds between carbon and sulfur in the polymer structure. [24,31] Furthermore, additional peaks were detected at 473 and 936 cm^{-1} that are associated with the ring stretching of the S–

S bonds. [24,31,40] Therefore, this corroborates that it does not correspond to S₈ elemental sulfur, but rather originates after the reaction of sulfur with PAN, demonstrating the formation of a short chain –S_n– ($n \leq 4$). [41] On the other hand, other authors show that the peak detected at 936 cm⁻¹ is associated with C–S and N–S covalent bonds, which is in agreement with the polymer SPAN structure. [33] Finally, in the SPAN spectrum, the most intense signals observed at 1345 and 1550 cm⁻¹ were assigned to the bands D and G of the carbonaceous materials, [22,24,42] and appeared in the Raman spectrum of pPAN. The value of the intensity ratio I_D/I_G was close to 1, which is indicative of the high structural disorder of the SPAN carbon, confirming the observations derived from the XRD study. In terms of Raman and IR spectra for PAN, it is observed that upon heating and reacting with sulfur, the asymmetric and symmetric CH₂ stretching (3000-2900 cm⁻¹), CH₂ bending (1454 cm⁻¹), and C-N triple bond stretching (2243 cm⁻¹) vanish. This suggests that PAN undergoes dehydrogenation and cyclization, contributing to the bands that indicate the bonding between sulfur and the matrix. [43]

Figure 1d illustrates the ATR-FTIR spectra of the samples. The sulfur spectrum presents some bands corresponding to the S₈ molecule below 600 cm⁻¹. [39,44] In contrast, the PAN spectrum shows several signals. In particular, the band at 2243 cm⁻¹ corresponds to the C-N triple bond, while the methylene group vibrations are represented by a signal at 1454 cm⁻¹ and a wide signal between 2900 and 3000 cm⁻¹, attributed to asymmetric/symmetric stretching and scissoring, respectively, as shown for the Raman spectra as well. [20] When PAN is subjected to the pyrolysis process, different bands are shown. The pPAN sample shows a predominant signal at 1580 cm⁻¹, corresponding to the vibration of the C=N–C=C conjugate bonds. At 1370 cm⁻¹ is the characteristic band of the vibration of the =C–H bond,

and at 1150 cm^{-1} the C–C and C–N bonds.^[33] Furthermore, at 801 cm^{-1} there is a band corresponding to the ring breathing indicative of PAN cyclisation. This same band is also found in the SPAN sample.^[31] Instead, other new signals appeared at lower wavenumbers.^[34] In the SPAN, several types of bands are detected, among which at 513 cm^{-1} there is a stretching band of the S–S bond, while at 670 cm^{-1} a band characteristic of the C–S covalent bond is detected, confirming the presence of this type of bond between the polymer chain and sulfur.^[22,45] Additionally, at 934 cm^{-1} a band corresponding to the stretching of the chain ring of the S–S and C–S side chains is detected. Furthermore, according to Huang et al.,^[46] they indicate that this band may also belong to N–S-type bonds, which is highly probable in the SPAN structure. The other predominant bands are part of the different types of C–C or C–N bonds of the polymer chain.^[45] Therefore, the thermal and structural analyses of SPAN have shown that, under the proposed synthesis conditions, PAN undergoes a vulcanisation process with sulfur, through dehydrogenation and partial carbonisation mechanisms. The structural formation of SPAN has been confirmed and the presence of physically confined sulfur is detected in the synthesised product.

The morphology and elemental mapping of the SPAN was investigated by SEM and EDS mapping, as shown in Figure 2a and Figure.S2, respectively. The SEM image shows an irregular morphology in the form of clusters with particles of different sizes. EDS mapping reveals that the elements carbon, sulfur, nitrogen, oxygen, and titanium are distributed homogeneously throughout the material. The textural properties of the materials that act as cathodes in Na–S batteries can play a relevant role in the electrochemical performance of the electrode.^[28,47] Figure 2b shows the nitrogen adsorption-desorption isotherms for the SPAN sample. According to the Brunauer-Deming-Deming-Teller (BDDT) classification, the shape

of the isotherm can be defined as a combination between type II and III, characteristic of non-porous and macroporous solids, which agrees with the morphology that could be observed in the SEM images. In this case, there is no Point B, so the formation of the monolayer is not identifiable since the interaction of the adsorbent-adsorbate is relatively weak and the adsorbed molecules are found around the most favourable sites on the surface. [48] However, the pore size distribution (inset of Figure 2b) obtained by density functional theory (DFT) shows the existence of mesopores around 20 nm, and pore diameters mostly between 40 – 50 nm. The specific surface area of the SPAN is only 5.3 m²/g and the total pore volume was 0.04 cm³/g. The macroporosity present in the material significantly enhances electrochemical performance. This is primarily due to the increased surface area provided by macroporous structures, which offers more active sites for electrochemical reactions, thus boosting energy storage and release efficiency. Additionally, the interconnected macropores facilitate faster and more efficient ion transport, reducing resistance, improving conductivity and maintains the electrode's integrity during charge-discharge cycles. [49,50] As a conclusion to the discussion of the morphology and textural properties of SPAN, this material can be considered dense, as reported by other authors. [25,51] The microporosity of the material is found between SPAN particles, so it is not associated with particles having their own pores, as observed in the SEM image. In this way, the active surface is the one found in the outer structure of each SPAN particle, which is useful in Na–S batteries. The sulfur is part of the polymer chain of the SPAN particle and EDS mapping shows a homogeneous sulfur distribution.

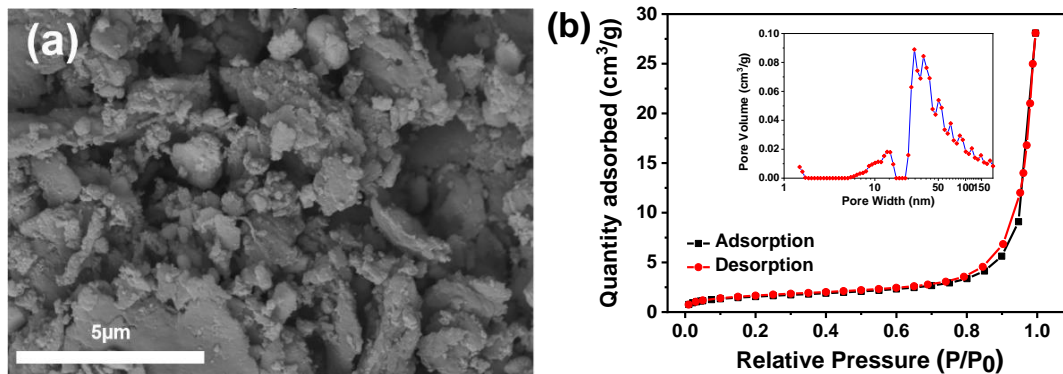


Figure 2. (a) SEM image of SPAN; and (b) Nitrogen adsorption-desorption isotherms of SPAN. Inset: pore size distribution.

To obtain information on the chemical composition of SPAN, x-ray photoelectron spectroscopy analysis was performed. Figure 3a shows the survey scan where the predominant signals corresponding to C $1s$ (284 eV), O $1s$ (~530 eV), S $2p$ (~163 eV), N $1s$ (~398 eV), and Ti $2p$ (~458 eV) regions are detected. In contrast, in the pPAN survey (Figure S3a) only signals corresponding to C $1s$ (~284 eV), O $1s$ (~530 eV), and N $1s$ (~398 eV) are observed. C $1s$ high-resolution XPS spectra of SPAN were deconvoluted into three clearly differentiated components associated with C=C/C–C (sp^2/sp^3 centres), C–N bonds and C–S bonds located at ca. 283.4, 285.4, and 287.3 eV, respectively, which confirms that C–S bonds exist in the polymer chain (Figure 3b).^[23,25] In addition, the XPS spectra of S $2p$ demonstrates that sulfur has bonded to the carbonaceous chain as a short-chain organosulfide, as shown in the S $2p_{3/2}$ region at 164 eV with double bonds, while the signal centred at 161 eV corresponds to C–S single bonds (Figure 3c).^[52] Furthermore, the existence of S–N bonds in the polymeric chain is demonstrated by the presence of a signal at 166.4 eV.^[33] The signal located at 168 eV corresponds to the C–SO_x bonds, indicating the presence of oxidising groups in the structure of SPAN.^[53] The N $1s$ signals reveals the two characteristic contributions corresponding to two different chemical environments for nitrogen. The signal

centred at 397.8 eV corresponds to pyridinic nitrogen, while pyrrolic nitrogen appears at 399.4 eV. [54,55] The latter is believed to enhance the conductivity of carbon by providing additional electrons to the delocalised π -system. [56,57] In the Ti $2p$ region a doublet corresponding to a spin-orbit splitting is observed (Figure S3b). The Ti $2p_{3/2}$ component is centred at 458 eV and is assigned to the Ti^{4+} oxidation state of TiO_2 . [58,59]

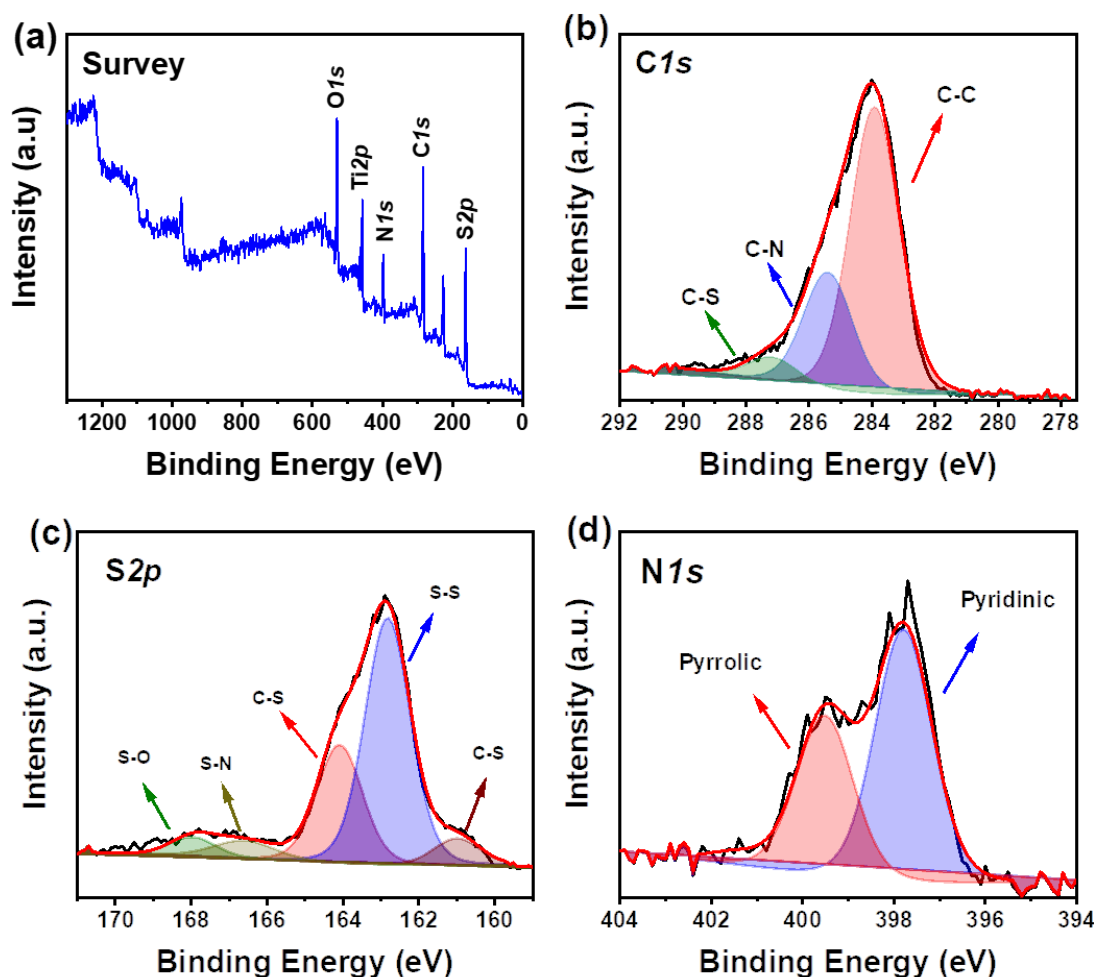


Figure 3. (a) XPS survey scan of SPAN; (b) XPS high resolution spectra of C $1s$; (c) S $2p$; and (d) N $1s$.

To date, there is some controversy regarding the molecular structure of SPAN, with some molecular models having been proposed. On the other hand, the results of the different structural characterisation techniques such as XPS, Raman, and ATR-FTIR studies confirm the feasible preparation of a SPAN doped with TiO_2 , the potential structure of which is illustrated in Figure 4. The proposed molecule has pyrrolic and pyridinic rings with different covalent bonds between C–S, C=S, N–S and short chains of a few S atoms in length. ^[19] The polymer matrix and metal oxide particles appear to be uniformly dispersed, based on what was observed by EDS elemental mapping. Furthermore, it can be argued that sulfur is present in SPAN in two ways, either through chemical interactions with covalent bonds to the SPAN matrix or by physical interactions between all components. Besides, TiO_2 remained physically adsorbed to the matrix. ^[21]

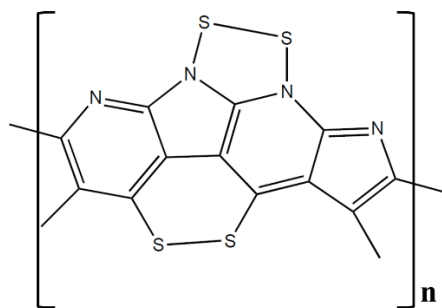


Figure 4. Potential structure proposed for SPAN sample.

2.2. Electrochemical properties

Since the sulfur is covalently bonded to the carbon backbone in the synthesised SPAN, long-chain polysulfide dissolution, which is responsible for the polysulfide shuttle effect and capacity fading, can be avoided. ^[29] In this way, the reactions that take place in the battery are quasi-solid-state conversion reactions, as they substantially eliminate the presence of long-chain sulfur polysulfides, forming reaction intermediates in a solid state. These

reactions are characteristic of cathodes in which sulfur is forming covalent bonds or physically confined in the polymeric chain of SPAN. [32,60]

Different electrochemical tests were performed to evaluate the behaviour of the SPAN as cathode in room-temperature Na–S cells. The Figure 5a shows the cyclic voltammetry (CV) curves at different scan rates from 0.1 to 0.5 mV/s. Figure S4 shows that the first cycle of the voltammetry was different from the others. However, the oxidation profile of the 1st cycle presented the same curve shape for the rest of the cycles. Instead, several notable peaks are detected in the cathodic branch. The first of them is found at 2 V, corresponding to long-chain polysulfides from physically confined sulfur that are irreversibly lost since they are not recorded again in the other cycles. The next signal begins at 1.6 V, referring to the formation of short chain polysulfides from the sulfur that is covalently bonded to the SPAN polymer chain. In the cathode branch below 1.3 V, the reduction step has much more capacity than the following curves. This may be due to the fact that sodiation produces an irreversible volume expansion that distorts the carbon structure, since the formation of Na₂S requires a volume expansion of ~271 vol.% to accommodate the carbon. [61] The initial geometric constraint on the carbon structure must be relaxed for an easy sodiation/desodiation cycle to occur impacting the first sodiation thermodynamic. Furthermore, the classical description of the formation of the solid electrolyte interphase (SEI) and electrolyte decomposition in these sodium systems occurs experimentally from 1.6 to 1.0 V vs. Na⁺/Na. [25,62] Starting from the first scan, all other CV curves have a similar shape. In the subsequent reduction scans, a wide peak is observed around 1.8 V, indicating the reduction of sulfur in the SPAN skeleton to form short-chain polysulfide intermediates, followed by the cleavage of S–S bonds at 1.2 V, and the formation of low-order polysulfides

NaS_n ($n \leq 4$) plus the final discharge product (Na_2S).^[29,40,63] In the oxidation scan, a broad peak is observed where two signals overlap. The first one located at 1.85 V and a small shoulder peak at about 2.15 V correspond to the reversible desodiation and the reconstruction of the S–S bonds.^[40,63,64] The diffusion coefficient of sodium ions (D_{Na^+}) was calculated by cyclic voltammetry (CV) using the Randles-Sevcik equation as described below to evaluate the rate at which ion transfer occurs through the electrochemical system.

$$I_p = 2.69 \cdot 10^5 n^{1.5} A D_{\text{Na}^+}^{0.5} \nu^{0.5} C_{\text{Na}^+} \quad (\text{Eq. 1})$$

Where I_p indicates the peak current (A), n is the number of electrons in the reaction, A is the electrode area (cm^2), ν is the scanning rate (V s^{-1}), and C_{Na^+} is the concentration of sodium ions in the electrolyte. In Figure 5b, two electrons were used for the anodic branch since both processes overlap in a single broad peak located at approximately 1.85 V. In the case of the cathodic branch, the process was best defined with a single electron. In both cases, the diffusion coefficient obtained were of the order of those reported in the literature, indicating rapid mobility of the Na^+ ion in the cathode, which is a key factor required for correct performance of the battery.^[16,24–26,29,64]

The impedance spectra shown in Figure 5c and 5d are represented with the Nyquist plots of the cell at open circuit voltage (OCV) and after four CV measurements, respectively. The intersection of the high-frequency semicircular arc with the Z_{real} axis signifies electrolyte resistance. However, at intermediate frequencies, the semicircular arc is associated with charge transfer resistance. As usual, both resistances decrease in the cell after cycling. Nevertheless, in this system the charge transfer resistance decreased notably after electrode activation (from 4500 to 70 Ω) induced by cathodic and anodic reactions, observed in the CV

curves after complete impregnation of the cathode with the electrolyte. This improvement facilitates the transference of sodium ions through the cell.^[29,65] This reduction in surface resistance indicates that the repeated breaking and reforming of the SEI layer results in a larger surface area, which helps reduce the energy required for stripping and plating. This phenomenon on Na-S batteries has been noted by other researchers.^[29] Furthermore, Figure S5 show the EIS spectra fitted to an equivalent circuit with the resistance values.

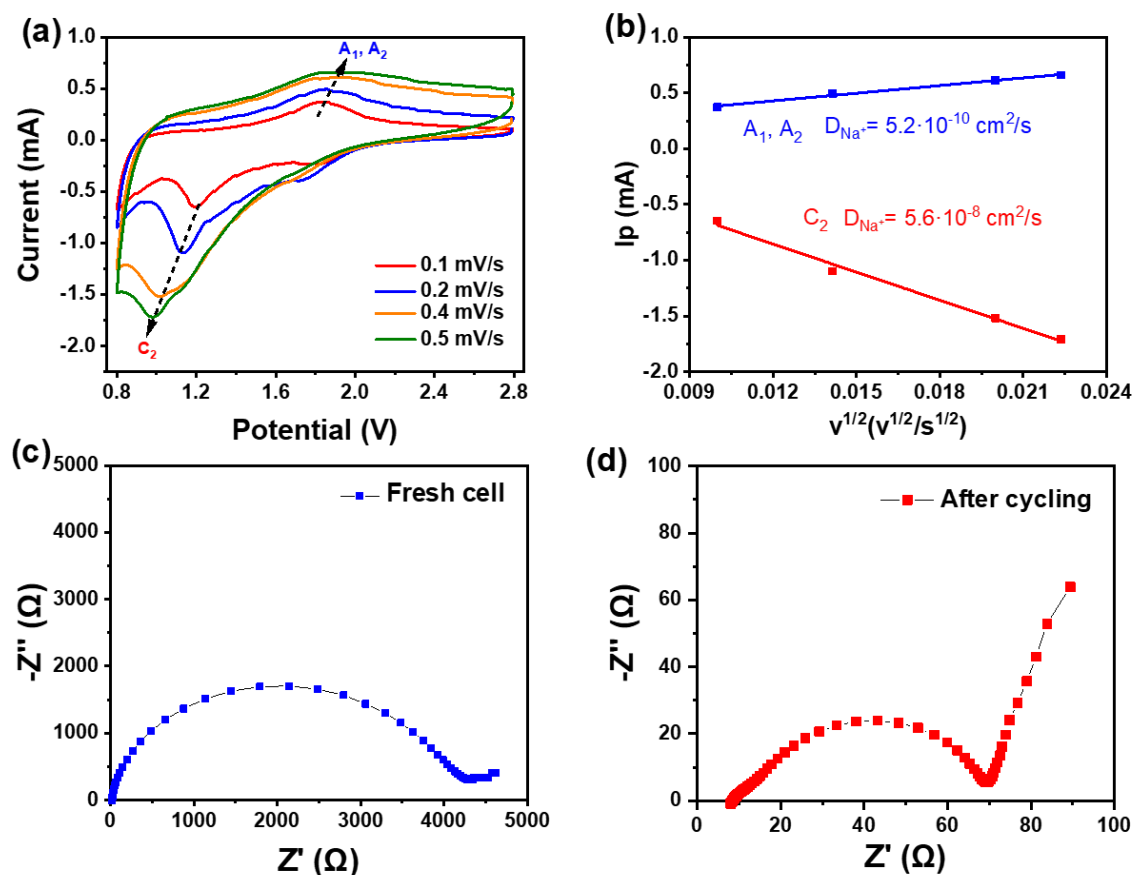


Figure 5. (a) CV measurements performed between 0.8 and 2.8 V vs Na^+/Na recorded at different scan rates for SPAN; (b) Representation of I_{peak} vs. $v^{1/2}$ for the calculation of the D_{Na^+} by Randles-Sevcik; (c) and (d) EIS at OCV and after cycling, respectively.

Galvanostatic charge and discharge curves were recorded within a potential range of 0.8 to 2.8 V, as illustrated in Figure 6a. In this way, typical profiles of quasi-solid-state reactions are recorded.^[66] At low rate, the profile shows a small plateau around 2 V that may correspond to confined sulfur or the reduction of sulfur in the SPAN skeleton to form short-chain polysulfide intermediates. It is noteworthy that as cycling rates increase, this plateau becomes less prominent. Moreover, a large plateau appeared at 1.2 V corresponding to the formation of the final discharge product (Na_2S). This plateau is consistently observed at all recorded cycling rates, except at very high rates such as 1C and 2C. It is important to highlight that the first cycle (Figure S6), similar to that recorded by CV, exhibits a plateau at 2.1 V and 1.6 V corresponding to long-chain polysulfides derived from physically confined sulfur and short-chain polysulfides originating from sulfur covalently bonded, respectively. The fact that the capacity is significantly higher compared to the theoretical capacity for sulfur cathodes may be attributed to various processes. This could be due to an irreversible capacity that likely arises from the SEI formation, electrolyte decomposition, and reduction of SPAN.^[26] The first cycle experiences capacity degradation and voltage hysteresis due to irreversible processes taking places at the anode, along with poor electrical contact between SPAN and the carbon particles.^[67] Furthermore, a marked capacity drop was observed during the initial cycles, which is characteristic of these kinds of systems. Some authors associate this fading with the loss of active material from the deposition of non-conductive material on the cathode. Nevertheless, there are other authors who highlight the impregnation of the electrode with the electrolyte and attribute it to the stabilisation of the cells, not becoming prominent until the fifth cycle.^[68,69] The reaction mechanism follows what is described in the literature for SPAN cathodes, confirming that carbon and TiO_2 are not active for sodiation/desodiation under the cycling conditions tested.^[70]

Figure 6b shows the behaviour of the cell during a multi-rate experiment (rate capability test). During the first five cycles at a low cycling rate of C/20, the capacity experiences a substantial drop during the discharges from 1400 to 1200 mAh/g_s. Subsequently, the cell was cycled at higher rates, producing excellent capacity values, and demonstrating high stability between charge and discharge cycles. Coulombic efficiency remains close to 100% at all cycling rates, underscoring the efficiency of the SPAN electrode. Remarkably, at high rates such as 1C and 2C, the cell delivers significant capacities at 500 and 400 mAh/g_s, demonstrating brilliant behaviour of the SPAN in this type of batteries. Finally, the cell was cycled again at a slow rate of C/20, exhibiting good performance and providing an average capacity value of approximately 800 mAh/g_s. The excellent recovery behaviour of the cell when returning to a lower rate is due to the good diffusion coefficients values, since the polymeric structure of the SPAN together with the electrolyte makes the Na⁺ ions diffuse through the cell with great facility during the charges and discharges. [22] In addition, the SPAN structure gives the cathode high conductivity due to the covalent bonds between the polymer structure and sulfur, which is in contrast with the conventional sulfur cathodes suffering from low conductivity. [22] The role of TiO₂ should be emphasised since it is reported in the literature that they are capable of trapping polysulfides. [21,34,59,70]

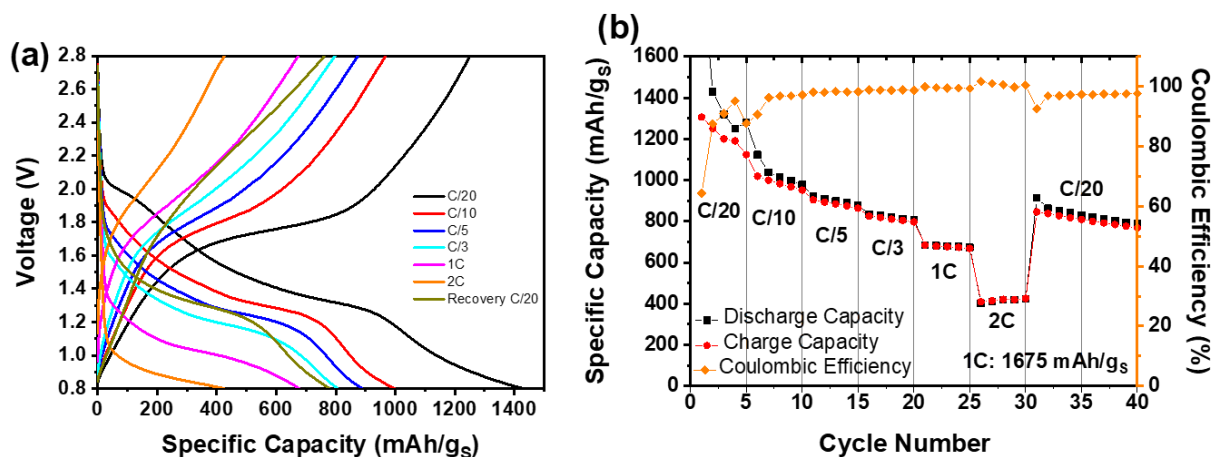


Figure 6. (a) Selected galvanostatic discharge/charge profiles of the rate capability test at different rates; (b) Rate capability test from C/20 to 2C and then back to C/20 rate.

The long-term cell cycling experiment was carried out at a moderate rate of C/10 and at double rate (C/5, 335 mA/g), employing galvanostatic charge and discharge cycles (Figure 7a). At C/10 rate, a significant stability with excellent capacity values was observed. Before cycling, some activation cycles were carried out at a low rate, as has been previously reported.^[71] The initial capacity values remained above 1100 mAh/g_s and after 100 cycles the specific capacity was 642 mAh/g_s, demonstrating stable behaviour with a capacity loss of 5.06 mAh/g_s per cycle (decay rate below 0.44% per cycle). When the rate was halved to a moderate rate of C/5, the cell delivered exceptional capacities during 100 charge/discharge cycles. In this case, a great initial capacity of 932 mAh/g_s was achieved, with a remarkable final specific capacity of 480 mAh/g_s and a capacity loss of 4.52 mAh/g_s per cycle (decay rate of 0.48% per cycle).

A long cycling test at C/5 rate is shown in Figure 7b. The performance of the SPAN electrode exhibited highly stable behaviour. In this experiment, the cycling result can be divided into two regions. The first region experiences a more pronounced capacity loss from

the 100th to the 400th cycle, starting with an initial specific capacity of 480 mAh/g_s and a capacity loss of 0.53 mAh/g_s per cycle (0.14% per cycle). The second region continues up to a thousand cycles with high stability and a capacity loss of 0.13 mAh/g_s per cycle (0.11% per cycle). These low values of capacity loss per cycle show great stability of the cell throughout the cycles thanks to the avoidance of the shuttle effect due to the type of polymer structure of SPAN with a network of covalent bonds and dopants that prevent the formation and dissolution of long-chain polysulfides.^[34] Furthermore, the suitability of the electrolyte is demonstrated without the need for additives that would make the synthesis process more expensive.^[40]

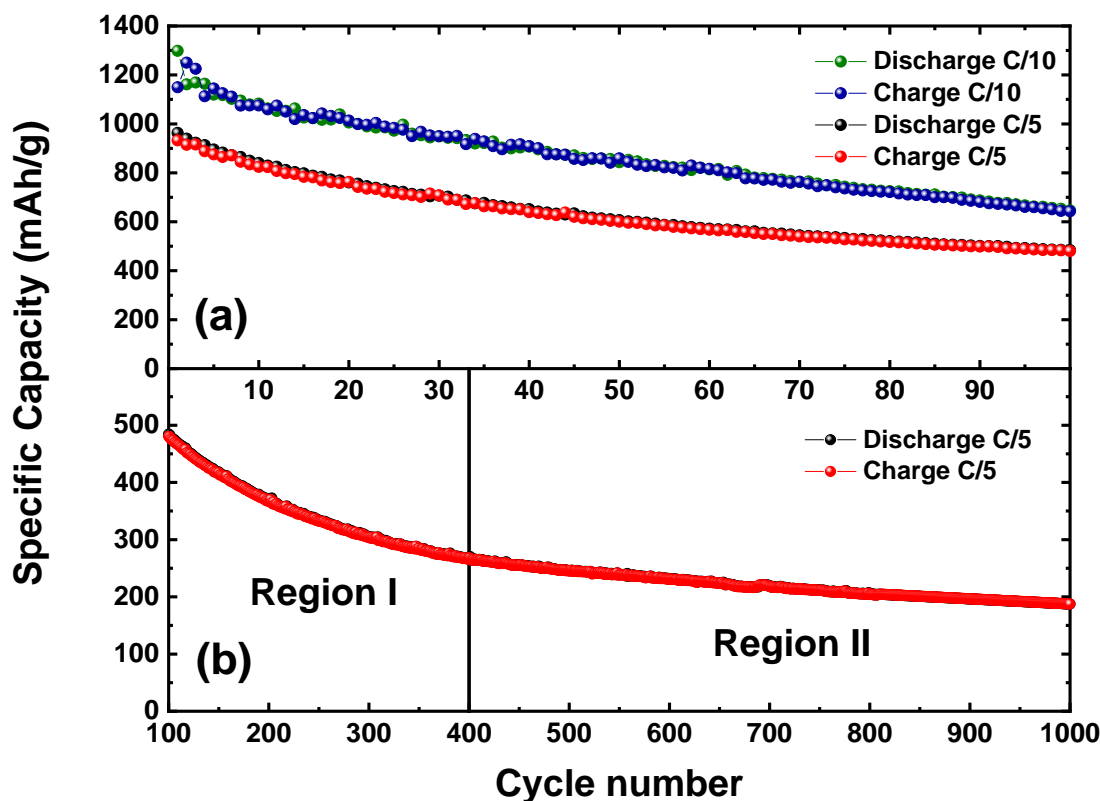


Figure 7. (a) Long-term charge/discharge capacity values at C/10 and C/5 rates; (b) ultra long-term charge/discharge at C/5 rate.

In order to compare the state of the cathode before cycling and after cycling, an SEM study is carried out and, in this way, evaluate and provide insights on the impact of cycling on the cathode. Figure S7a shows the cathode before cycling in which a homogeneous morphology is observed with particles of different sizes without cracks. SEM images of post-mortem SPAN electrodes after cycling are depicted in Figure S7b and S7c. In both cases, it is evident that the morphology of the cathode material remains devoid of cracks or clusters that hinder connectivity among electroactive particles, thereby enabling them to continue fulfilling their function for a prolonged period.

In Table S1, the synthesis conditions, active material contents, and electrochemical performance of different SPAN-type materials used as cathodes for sodium-sulfur batteries are shown for comparative purposes. It is noteworthy that the literature reports great results in terms of capacity and cyclability. Nevertheless, in most cases, SPAN synthesis involves complex and expensive methods such as electrospinning.^[28] Hence, it should be emphasised that this study employs rapid and straightforward synthesis approaches, offering advantage in cost-effectiveness and scalability for prospective applications. This contrasts with more complex processes used in preparing Na-S cathodes, which involve high energy consumption and multiple reaction stages. Furthermore, it can be observed that the material proposed in this study exhibits high stability over a thousand charge/discharge cycles. In the literature, only Murugan et al.^[29] and Wang et al.^[27] achieved such a high cycle life. However, these authors prepared the cathode incorporating 20% by weight of conductive agent (acetylene black or carbon Super P) and employed an unusual cell composition. The first author used an unconventional electrolyte where they themselves synthesized the sodium salt (Na[B(hfip)₄]), associated with significant synthesis challenges, and

incorporating 13% by weight of the FEC additive. While Wang et al. [27] utilised nickel foam as a current collector, thereby substantially increasing the cost of scaling up its configurations and lowering the energy density of the cell by notably increasing the weight of the current collector.

Therefore, it could be concluded that the good electrochemical performance of the SPAN cathodes reported here can be attributed to the activation process, resulting in the optimisation of the structure and the formation of a protective and stable cathode electrolyte interphase (CEI). Additionally, the presence of various nitrogen species in the structure enhances the ability to anchor sodium polysulfides as well as dopants. Besides, the presence of TiO₂ further facilitates the sodiation/desodiation process due to the synergistic effect of TiO₂ and the solid-solid mechanism of SPAN. Furthermore, it is noteworthy that the cathode preparation involved only 10% conductive agent and excluded high-cost additives like FEC, which are known to enhance electrochemical performance. This approach was adopted to reduce raw material consumption and lower overall costs. These characteristics of the SPAN-based cathode synthesised in this study lead to excellent long-term performance, showing an average capacity loss lower than 0.12%. This behaviour improves the values reported for more complex SPAN cathodes, where losses of 0.23% are reported in prolonged cycling of Na–S cells. [40]

3. Conclusions

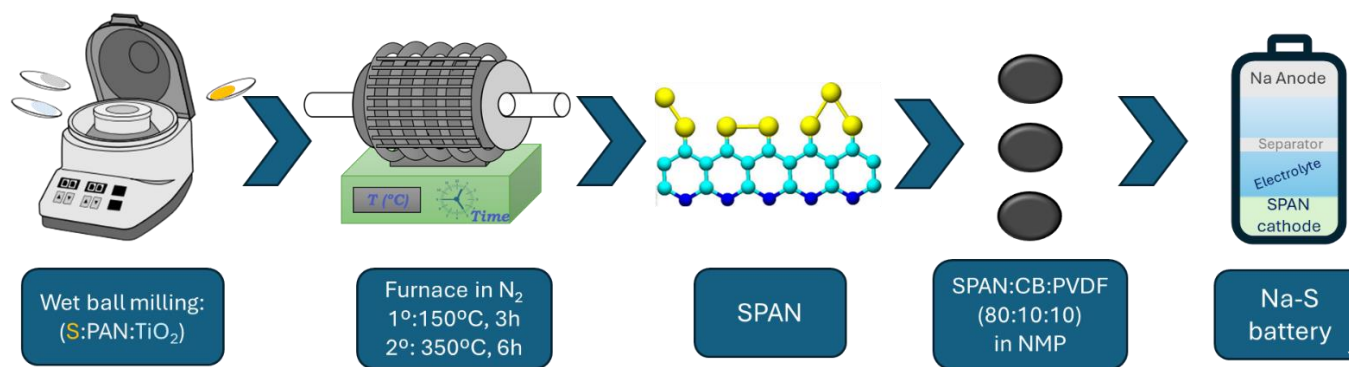
In summary, a sulfurised polyacrylonitrile (SPAN) has been successfully synthesised through a non-complex method for use as cathodes in RT Na–S batteries. A high retained sulfur content is achieved through covalent bonds between sulfur and nitrogen, and the carbon chain are formed in the polymeric structure of SPAN, thereby preventing the shuttle

effect. Suitable diffusion coefficients are achieved that allow the rapid migration of Na⁺ ions, enabling a remarkable electrochemical performance, without the need to increase the proportion of the activating agent or add high-cost additives to the electrolyte. The unique property of the material enables reversible charge and discharge capabilities of 1200 mAh/g_s, besides exhibiting excellent performance over an ultra-long cycling of up to 1000 cycles, with a capacity loss of 0.11% per cycle, and suitable behaviour at higher currents of up to 2C. Therefore, this study could offer a new perspective for designing room-temperature Na-S batteries with improved performance.

4. Experimental section

4.1. SPAN preparation

Sulfur powder (99% Biopack), polyacrylonitrile (PAN, Polysciencies, Inc.), and TiO₂ nanoparticles were combined with ethanol in a mass ratio of 4:1:0.5, using a planetary ball mill (Retsch, PM 100) at 300 RPM for three hours. Briefly, 2 g of S was mixed with 0.5 g of PAN and 0.25 g of TiO₂. After mechanical treatment, the mixture underwent a two-step heating process in a tube furnace (Indef, T-150 model) at 150 °C for 3 hours, followed by 350 °C for 6 hours (ramp of 5 °C/min) under a flow of nitrogen gas at 100 mL/min to produce 1 g of SPAN sample. To elucidate the structural characterisation of SPAN, a pPAN sample has been synthesised, which consists of carrying out the same pyrolysis process but only for the PAN precursor.



Scheme 1. Synthesis of SPAN and fabrication of SPAN cathodes for Na-S batteries

4.2. Cathode preparation

Cathode electrodes were prepared by mixing 80 wt.% SPAN and 10 wt.% polyvinylidene fluoride (PVDF, Sigma-Aldrich) as binder, and 10 wt.% Super P carbon (SPC, Tymcal) as conductive agent in N-methyl-2-pyrrolidone (NMP, Sigma-Aldrich) as solvent to form the electrodic mixture or slurry. The slurry was cast on carbon cloth (GDL, ELAT LT1400W) using the doctor blade coating technique and the electrodes were dried in an oven at 60 °C for 24 h. After that, the electrodes were cut into discs of 13 mm diameter and dried again at 45 °C for 3 h under vacuum in a glass oven (Buchi, B-585). The sulfur mass in all cells is ~1 mg/cm².

4.3. Structural, textural, morphological, and compositional characterisation

Thermogravimetric analysis data were recorded using a Mettler Toledo TGA/DSC instrument. The samples were analysed under an inert atmosphere using heating conditions from 30 to 900 °C at a ramp rate of 5 °C/min and under a helium flow rate of 50 mL/min. The thermobalance has a Pfeiffer Vacuum Mass Spectrometer, model ThermoStar TM GSD 320, coupled to the output. Elemental analysis (EA) was recorded using a LECO 928 macroanalyzer. The sample was introduced into the analyser's combustion oven, maintained

at a temperature of 1350°C, in conjunction with a defined volume of oxygen. The resulting gases were transported by an inert gas (helium) to a chromatographic column, where they were separated and detected by a thermal conductivity detector. Attenuated total reflection (ATR) Fourier transform infrared (FTIR) spectroscopy was performed on a Perkin-Elmer Spectrum Two. Spectra were collected with a spectral window of 3500 – 500 cm⁻¹ using 4 cm⁻¹ resolution and accumulating 64 scans. X-ray diffraction patterns were recorded with a D8 Discover A25 (Bruker) diffractometer using monochromatic Cu K α (1.5406 Å) radiation. The diffraction data was obtained using a range of 5 – 80° (2 θ) with a step size of 0.040° and a rate of 1.05 s per step. Raman spectra were obtained with a Renishaw Raman Instrument (InVia Raman Microscope), which was equipped with a Leica microscope consisting of various lenses, monochromators, filters, and a CCD camera using a green laser light excitation source (532 nm). A total of 20 scans per spectrum were acquired with 10 s of exposure time and a laser power of 0.1% over the maximum provided. X-ray photoelectron spectroscopy (XPS) was carried out with a SPECS PHOIBOS 150 MCD spectrometer using monochromatic Mg K α (1253.6 eV) radiation and a multichannel detector. Data analysis was performed using Casa XPS software. The nitrogen adsorption/desorption data were recorded with a Micromeritics ASAP 2020 system at liquid nitrogen temperature (77K) using nitrogen gas as an adsorbate. The pore size distribution was calculated by the density functional theory (DFT) method applied to the adsorption branch isotherm. The morphology of the samples was studied by scanning electron microscopy (SEM), and EDS elemental microanalysis with a Helios Nanolab 650 (FEI Europe B.V).

4.4. Cell assembly and electrochemical characterisation

Sodium-sulfur batteries were prepared in CR2032 coin-type cells and assembled inside an argon-filled glovebox (Inert model IL-4GB) with oxygen and humidity levels <0.1 ppm and < 0.5 ppm, respectively. The cells were composed of the previously prepared cathode as the working electrode, and sodium metal as counter and reference electrodes. The sodium foil was prepared by crushing and punching it into a disk of 14 mm. The electrolyte formulation was an anhydrous 1 M NaClO₄ salt (Stem Chemicals) dissolved in a 1:1 (v:v) mixture of ethylene carbonate (EC, Sigma-Aldrich) and propylene carbonate (PC, Sigma-Aldrich). Glass fibre (GF/F Whatman) was used as separator, with its thickness and porosity being 400 μ m and 0.6 μ m, respectively.

The electrochemical study was performed by galvanostatic measurements using a potentiostat-galvanostat Neware BTS 4000 working with a voltage window of 0.8 – 2.8 V vs Na⁺/Na. In the long-term galvanostatic experiments, the current density was calculated from the theoretical sulfur capacity, corresponding 1C with 1675 mA/g_s. The cyclic voltammetry (CV) was conducted in a Solartron-1286, and electrochemical impedance (EIS) measurements were carried out using an Autolab PGSTAT-204 instrument. CV curves were recorded at different scan rates (0.1, 0.2, 0.4, and 0.5 mV/s) with a potential window from 0.8 to 2.8 V. EIS spectra were measured in open circuit voltage (OCV) and after CV cycles in the frequency range of 500 kHz to 0.1 Hz at a disturbance amplitude of 10 mV. The simulation program used to fit the equivalent circuit was Zview 2 Scribner Associates.

Acknowledgements

This research was funded by Spanish Ministry of Science and Innovation MCIN/AEI/10.13039/501100011033 and the European Union “NextGenerationEU/PRTR”

(Projects PID2023-147080OB-I00, PID2020-113931RB-I00 & PDC2021-120903-I00); “*Juan de la Cierva – Incorporación*” fellowship (IJC2020-045041-I), Cordoba University (*Plan Propio de Investigación 2023, UCOLIDERA*), and Junta de Andalucía (FQM-175 Group). AYT thanks to CONICET program “Ayudas para la recualificación del sistema universitario español, Modalidad María Zambrano” and projects “Iniciativa Federal para el Desarrollo de Materiales y Procesos Sustentables para el Almacenamiento de Energía, EX-2023-42139041--APN-DDYGD#MCT” and CONICET-PIP 2021-2023 GI - 11220200100704CO. The authors wish to acknowledge the technical staff from the *Instituto Químico para la Energía y el Medioambiente (IQUEMA)* and *Servicio Central de Apoyo a la Investigación (SCAI)* of Córdoba University.

Conflict of interest

The authors declare no conflict of interest.

References

- [1] R. Van Noorden, *Nature* **2014**, *507*, 26–28.
- [2] S. Chung, A. Manthiram, *Adv. Mater.* **2019**, *31*, 1901125.
- [3] L. Ma, Y. Lv, J. Wu, Y. Chen, Z. Jin, *Adv. Energy Mater.* **2021**, *11*, 2100770.
- [4] X. Yu, A. Manthiram, *Adv. Funct. Mater.* **2020**, *30*, 2004084.
- [5] D. Kumar, S. K. Rajouria, S. B. Kuhar, D. K. Kanchan, *Solid State Ionics* **2017**, *312*, 8–16.
- [6] X. Yu, A. Manthiram, *Matter* **2019**, *1*, 439–451.
- [7] L. Lin, C. Zhang, Y. Huang, Y. Zhuang, M. Fan, J. Lin, L. Wang, Q. Xie, D. Peng, *Small* **2022**, 2107368.
- [8] S. Zhang, Y. Yao, Y. Yu, *ACS Energy Lett.* **2021**, *6*, 529–536.
- [9] X. Ye, S. Luo, Z. Li, J. Ruan, Y. Pang, J. Yang, J. Wang, S. Zheng, *J. Energy Chem.* **2023**, *86*, 620–627.
- [10] I. Kim, C. H. Kim, S. hwa Choi, J.-P. Ahn, J.-H. Ahn, K.-W. Kim, E. J. Cairns, H.-J. Ahn, *J. Power Sources* **2016**, *307*, 31–37.
- [11] Y. Yao, L. Zeng, S. Hu, Y. Jiang, B. Yuan, Y. Yu, *Small* **2017**, *13*, 1603513.
- [12] A. Y. Tesio, J. de Haro Niza, L. M. Sanchez, A. Rodríguez, A. Caballero, *J. Energy Storage* **2023**, *67*, 107627.
- [13] C. Hernández-Rentero, R. Córdoba, N. Moreno, A. Caballero, J. Morales, M. Olivares-Marín, V. Gómez-Serrano, *Nano Res.* **2018**, *11*, 89–100.
- [14] R. Zou, W. Liu, F. Ran, *InfoMat* **2022**, *4*, DOI 10.1002/inf2.12319.
- [15] Y. Wu, L. Wu, S. Wu, Y. Yao, Y. Feng, Y. Yu, *Small Sci.* **2021**, *1*, DOI 10.1002/smsc.202100059.
- [16] S. Li, Z. Zeng, J. Yang, Z. Han, W. Hu, L. Wang, J. Ma, B. Shan, J. Xie, *ACS Appl. Energy Mater.* **2019**, *2*, 2956–2964.

- [17] H.-C. Lin, J.-L. Hong, *ACS Appl. Energy Mater.* **2022**, *5*, 11304–11316.
- [18] J. Wang, J. Yang, J. Xie, N. Xu, *Adv. Mater.* **2002**, *14*, 963–965.
- [19] X. Zhao, C. Wang, Z. Li, X. Hu, A. Abdul Razzaq, Z. Deng, *J. Mater. Chem. A* **2021**, *9*, 19282–19297.
- [20] A. L. Páez Jerez, D. M. Chemes, E. L. Sham, L. E. Davies, A. Y. Tesio, V. Flexer, *ChemistrySelect* **2020**, *5*, 5465–5472.
- [21] A. L. Páez Jerez, L. E. Davies, A. Y. Tesio, V. Flexer, *J. Electrochem. Soc.* **2021**, *168*, 120536.
- [22] T. H. Hwang, D. S. Jung, J.-S. Kim, B. G. Kim, J. W. Choi, *Nano Lett.* **2013**, *13*, 4532–4538.
- [23] Z. Li, J. Zhang, Y. Lu, X. W. (David) Lou, *Sci. Adv.* **2018**, *4*, DOI 10.1126/sciadv.aat1687.
- [24] L. Wang, X. Chen, S. Li, J. Yang, Y. Sun, L. Peng, B. Shan, J. Xie, *J. Mater. Chem. A* **2019**, *7*, 12732–12739.
- [25] V. H. Pham, J. A. Boscoboinik, D. J. Stacchiola, E. C. Self, P. Manikandan, S. Nagarajan, Y. Wang, V. G. Pol, J. Nanda, E. Paek, D. Mitlin, *Energy Storage Mater.* **2019**, *20*, 71–79.
- [26] S. Murugan, S. V. Klostermann, P. Schützendübe, G. Richter, J. Kästner, M. R. Buchmeiser, *Adv. Funct. Mater.* **2022**, *32*, 2201191.
- [27] J. Wang, J. Yang, Y. Nuli, R. Holze, *Electrochem. commun.* **2007**, *9*, 31–34.
- [28] L. Zeng, Y. Yao, J. Shi, Y. Jiang, W. Li, L. Gu, Y. Yu, *Energy Storage Mater.* **2016**, *5*, 50–57.
- [29] S. Murugan, S. Niesen, J. Kappler, K. Küster, U. Starke, M. R. Buchmeiser, *Batter. Supercaps* **2021**, *4*, 1636–1646.
- [30] P. Hu, F. Xiao, Y. Wu, X. Yang, N. Li, H. Wang, J. Jia, *Chem. Eng. J.* **2022**, *443*, 136257.

- [31] K. Yu, G. Cai, M. Li, J. Wu, V. Gupta, D. J. Lee, J. Holoubek, Z. Chen, *ACS Appl. Mater. Interfaces* **2023**, *15*, 43724–43731.
- [32] C. Y. J. Lim, Z. W. Seh, *Batter. Energy* **2022**, *1*, DOI 10.1002/bte2.20220008.
- [33] M. A. Weret, C.-F. Jeffrey Kuo, T. S. Zeleke, T. T. Beyene, M.-C. Tsai, C.-J. Huang, G. B. Berhe, W.-N. Su, B.-J. Hwang, *Energy Storage Mater.* **2020**, *26*, 483–493.
- [34] A. L. Páez Jerez, M. L. Vera, E. L. Sham, A. Y. Tesio, V. Flexer, *Electrochim. Acta* **2023**, *463*, 142876.
- [35] J. Fanous, M. Wegner, J. Grimminger, M. Rolff, M. B. M. Spera, M. Tenzer, M. R. Buchmeiser, *J. Mater. Chem.* **2012**, *22*, 23240.
- [36] M. Yu, Y. Xu, C. Wang, B. Zhu, Y. Wang, X. Hu, X. Lin, *J. Appl. Polym. Sci.* **2012**, *124*, 5172–5179.
- [37] A. Benítez, D. Di Lecce, G. A. Elia, Á. Caballero, J. Morales, J. Hassoun, *ChemSusChem* **2018**, *11*, 1512–1520.
- [38] T. Mahalingam, C. Selvakumar, E. Ranjith Kumar, T. Venkatachalam, *Phys. Lett. A* **2017**, *381*, 1815–1819.
- [39] B. A. Trofimov, L. M. Sinegovskaya, N. K. Gusarova, *J. Sulfur Chem.* **2009**, *30*, 518–554.
- [40] D. Liu, Z. Li, X. Li, X. Chen, Z. Li, L. Yuan, Y. Huang, *ACS Appl. Mater. Interfaces* **2022**, *14*, 6658–6666.
- [41] S. Li, Z. Han, W. Hu, L. Peng, J. Yang, L. Wang, Y. Zhang, B. Shan, J. Xie, *Nano Energy* **2019**, *60*, 153–161.
- [42] M. Lubas, J. J. Jasinski, M. Sitarz, L. Kurpaska, P. Podsiad, J. Jasinski, *Spectrochim. Acta Part A Mol. Biomol. Spectrosc.* **2014**, *133*, 867–871.
- [43] E. Cipriani, M. Zanetti, P. Bracco, V. Brunella, M. P. Luda, L. Costa, *Polym. Degrad. Stab.* **2016**, *123*, 178–188.
- [44] A. Shukla, A. K. Prasad, S. Mishra, A. Vinod, A. K. Varma, *Minerals* **2023**, *13*, 634.

- [45] X. Yu, J. Xie, J. Yang, H. Huang, K. Wang, Z. Wen, *J. Electroanal. Chem.* **2004**, *573*, 121–128.
- [46] C.-J. Huang, J.-H. Cheng, W.-N. Su, P. Partovi-Azar, L.-Y. Kuo, M.-C. Tsai, M.-H. Lin, S. Panahian Jand, T.-S. Chan, N.-L. Wu, P. Kaghazchi, H. Dai, P. M. Bieker, B.-J. Hwang, *J. Power Sources* **2021**, *492*, 229508.
- [47] W. Du, Q. Xu, R. Zhan, Y. Zhang, Y. Luo, M. Xu, *Mater. Lett.* **2018**, *221*, 66–69.
- [48] M. Thommes, K. Kaneko, A. V. Neimark, J. P. Olivier, F. Rodriguez-Reinoso, J. Rouquerol, K. S. W. Sing, *Pure Appl. Chem.* **2015**, *87*, 1051–1069.
- [49] S. Chaudhari, S. Y. Kwon, J.-S. Yu, *RSC Adv.* **2014**, *4*, 38931–38938.
- [50] Y. Zhang, S. Yu, G. Lou, Y. Shen, H. Chen, Z. Shen, S. Zhao, J. Zhang, S. Chai, Q. Zou, *J. Mater. Sci.* **2017**, *52*, 11201–11228.
- [51] L. Zhang, W. Zhang, Z. Zhu, Q. Huang, X. Liu, M. Zhang, W.-B. Pei, J. Wu, *J. Solid State Chem.* **2021**, *301*, 122359.
- [52] X. Wang, T. Gao, F. Han, Z. Ma, Z. Zhang, J. Li, C. Wang, *Nano Energy* **2016**, *30*, 700–708.
- [53] F. Luna-Lama, A. Caballero, J. Morales, *Sustain. Energy Fuels* **2022**, *6*, 1568–1586.
- [54] C.-J. Huang, K.-Y. Lin, Y.-C. Hsieh, W.-N. Su, C.-H. Wang, G. Bruncklaus, M. Winter, J.-C. Jiang, B. J. Hwang, *ACS Appl. Mater. Interfaces* **2021**, *13*, 14230–14238.
- [55] R. He, Y. Li, S. Wei, H. Liu, S. Zhang, N. Han, H. Liu, X. Wang, X. Zhang, *J. Alloys Compd.* **2022**, *919*, 165838.
- [56] J. Shan, Y. Liu, Y. Su, P. Liu, X. Zhuang, D. Wu, F. Zhang, X. Feng, *J. Mater. Chem. A* **2016**, *4*, 314–320.
- [57] Z. R. Ismagilov, A. E. Shalagina, O. Y. Podyacheva, A. V. Ischenko, L. S. Kibis, A. I. Boronin, Y. A. Chesalov, D. I. Kochubey, A. I. Romanenko, O. B. Anikeeva, T. I. Buryakov, E. N. Tkachev, *Carbon N. Y.* **2009**, *47*, 1922–1929.
- [58] J. Wu, S. Li, P. Yang, H. Zhang, C. Du, J. Xu, K. Song, *J. Alloys Compd.* **2019**, *783*,

- 279–285.
- [59] T. Lei, Y. Xie, X. Wang, S. Miao, J. Xiong, C. Yan, *Small* **2017**, *13*, DOI 10.1002/sml.201701013.
- [60] H. Liu, W. Lai, Y. Lei, H. Yang, N. Wang, S. Chou, H. K. Liu, S. X. Dou, Y. Wang, *Adv. Energy Mater.* **2022**, *12*, 2103304.
- [61] Y. Wang, W. Lai, S. Chou, H. Liu, S. Dou, *Adv. Mater.* **2020**, *32*, DOI 10.1002/adma.201903952.
- [62] S. Wei, S. Xu, A. Agrawal, S. Choudhury, Y. Lu, Z. Tu, L. Ma, L. A. Archer, *Nat. Commun.* **2016**, *7*, 11722.
- [63] S. Murugan, S. V. Klostermann, W. Frey, J. Kästner, M. R. Buchmeiser, *Electrochem. commun.* **2021**, *132*, 107137.
- [64] A. Y. S. Eng, D.-T. Nguyen, V. Kumar, G. S. Subramanian, M.-F. Ng, Z. W. Seh, *J. Mater. Chem. A* **2020**, *8*, 22983–22997.
- [65] X. Xu, D. Zhou, X. Qin, K. Lin, F. Kang, B. Li, D. Shanmukaraj, T. Rojo, M. Armand, G. Wang, *Nat. Commun.* **2018**, *9*, 3870.
- [66] H. Liu, W. Lai, Y. Lei, H. Yang, N. Wang, S. Chou, H. K. Liu, S. X. Dou, Y. Wang, *Adv. Energy Mater.* **2022**, *12*, DOI 10.1002/aenm.202103304.
- [67] S. Zhang, *Energies* **2014**, *7*, 4588–4600.
- [68] A. Manthiram, S.-H. Chung, C. Zu, *Adv. Mater.* **2015**, *27*, 1980–2006.
- [69] Á. Bonilla, A. Benítez, J. L. Gómez-Cámer, Á. Caballero, *J. Alloys Compd.* **2023**, *968*, 171810.
- [70] X. Ye, Z. Li, H. Sun, M. Wu, Z. An, Y. Pang, J. Yang, S. Zheng, *New Carbon Mater.* **2022**, *37*, 1116–1122.
- [71] X. Huang, J. Liu, Z. Huang, X. Ke, L. Liu, N. Wang, J. Liu, Z. Guo, Y. Yang, Z. Shi, *Electrochim. Acta* **2020**, *333*, 135493.

TOC:

Sulfurised polyacrylonitrile (SPAN) has been synthesized using a simple and scalable method, achieving a high sulfur content covalently linked to its framework. The development of SPAN cathodes demonstrates significant improvements in combating capacity fading and the shuttle effect in sodium-sulfur (Na-S) batteries. Additionally, these cathodes have demonstrated high stability up to 1000 cycles, reaching 400 mAh/g_s at a high rate of 2C.

